Chinese Chemical Letters 34 (2023) 107980

Contents lists available at ScienceDirect

Chinese Chemical Letters

journal homepage: www.elsevier.com/locate/cclet

A chiral lead-free tin(IV)-based halide organic-inorganic semiconductor with dielectric switching and phase transition

Hang Peng[1], Qin Liu[1], Yuhua Liu, Yanzi Lu, Weiqiang Liao*

Ordered Matter Science Research Center, Nanchang University, Nanchang 330031, China

ARTICLE INFO

Article history:
Received 14 September 2022
Revised 18 October 2022
Accepted 2 November 2022
Available online 4 November 2022

Keywords:
Lead-free
Chirality
Organic-inorganic metal halides
Dielectric switch
Phase transition

ABSTRACT

Chiral organic-inorganic metal halide semiconductors (OIMHSs) have recently attracted numerous interests due to their unique chirality, structural tunability, and extensive physical properties. However, most reported chiral OIMHSs contain toxic lead, which will be a potential obstacle to their further applications. Herein, we successfully synthesized a novel chiral lead-free tin(IV)-based OIMHS [(*R*)-3-hydroxyquinuclidinium]$_2$SnCl$_6$ ([*R*-HQ]$_2$SnCl$_6$). It exhibits a wide band gap (E_g) of about 4.11 eV. Moreover, [*R*-HQ]$_2$SnCl$_6$ undergoes a phase transition around 330 K (T_c) and shows distinct dielectric switching characteristics with good repeatability. This work enriches the chiral lead-free OIMHS family and stimulates further exploration of chiral lead-free OIMHS switching materials

Organic-inorganic metal halide semiconductors (OIMHSs) have gained immense attention over the past decades owing to their remarkable optical, electrical, and optoelectronic properties [1–4]. Among them, chiral OIMHSs have recently become particularly attractive for their unique chirality. Chiral OIMHSs could be constructed by employing chiral organic cations and semiconducting metal halides [5–7]. Through the interaction of chiral organic cations with inorganic frameworks, the chirality will be transferred to the hybrid structure [8–10]. Benefiting from this, chiral OIMHSs exhibit some fascinating physical properties, such as chiro-spintronics, circularly polarized luminescence, nonlinear optical property, and ferroelectricity [11–19]. For instance, Sargent and co-workers have realized the control of spintronic absorption and circularly polarized photoluminescence in chiral perovskites (*R*/*S*-methylbenzylammonium)$_2$(methylammonium)Pb$_2$Br$_7$ [11]. Xu *et al.* fabricated chiral OIMHSs (*R*/*S*)-(methylphenethylammonium)$_{1.5}$PbBr$_{3.5}$(DMSO)$_{0.5}$ based nanowires, which show circularly polarized second harmonic generation [18]. Moreover, the incorporation of chirality also greatly increases the possibility of inducing ferroelectricity in OIMHSs, which is one of the vital ideas of recently developed ferroelectrochemistry [19]. For example, chiral OIMHSs [*R*/*S*-1-(4-chlorophenyl)ethylammonium]$_2$PbI$_4$ crystalize in a chiral non-centrosymmetric space group *P*1 showing ferroelectricity, while their racemate adopts a centrosymmetric space group $P2_1/c$ without ferroelectricity [20]. Much progress has been made to broaden the chiral OIMHS family, however, chiral OIMHSs are still not abundant, and mainly of them are based on lead halides. Lead is a highly toxic element with adverse effects on human and biological systems, which has become a stumbling block on the road to the practical application of chiral OIMHSs. Therefore, it is highly desirable and urgent to develop chiral lead-free OIMHSs.

Benefiting from the superior structural tunability, the inorganic framework of OIMHSs can be rationally modulated. Based on this, researchers have been seeking low-toxic metal halides to replace lead-based ones. For example, by using the antimony and bismuth halides, Heine et al. synthesized chiral Sb-based and Bi-based OIMHSs, [(*R*)−1-(4-fluoro)-phenylethylammonium]$_4$[E$_2$X$_{10}$] (E = Sb and Bi; X = Cl, Br and I), respectively, which show efficient optical second-harmonic generation response. Despite many efforts that have been made to construct lead-free chiral OIMHSs in the past years [21–26], the resulting fruits were minimal. Tin and lead elements belong to the same group (IVA) in the periodic table and have similar outer electronic structures (ns^2np^2), which are important for optoelectronic features [27–32]. In addition, Sn^{2+} (1.35 Å) and Pb^{2+} (1.49 Å) have a similar ionic radius, inducing no obvious perturbation in the lattice structure [28]. But Sn^{2+} is easily oxidized to Sn^{4+}, leading to self-doping, which is the primary issue that inhibits the further development of Sn-based OIMHSs. In contrast to Sn^{2+}, Sn^{4+} is chemically stable. Therefore, Sn(IV)-based halides are expected to be promising alternatives for lead-based OIMHSs. Nevertheless, chiral Sn(IV)-based OIMHSs have been rarely explored.

* Corresponding author.
E-mail address: liaowq@ncu.edu.cn (W. Liao).
[1] These authors contributed equally to this work.

https://doi.org/10.1016/j.cclet.2022.107980
1001-8417/

Switching materials, whose physical properties can be switched between two relatively stable states under external stimuli (such as temperature, stress, electric field, and light), have attracted increasing interest due to their broad application foreground in the field of information technology [33–38]. Among them, dielectric switching between high and low dielectric states has potential applications in sensors, oscillators, and actuators [39–41]. It is found that in phase transition materials, the dielectric response usually undergoes an abrupt change around the phase transition temperature, which offers great opportunities for realizing the dielectric switching [42,43]. Structurally, the cavities formed by the inorganic parts of OIMHSs provide enough space for the order-disorder transition of organic cations under the temperature stimulus, favorable for inducing phase transitions. Some lead-based OIMHSs including chiral ones have been found to show phase transition and dielectric switching, such as trimethyliodomethylammonium lead trichloride [44], [benzyl-(2-fluoro-ethyl)-dimethyl-ammonium]$PbBr_3$ [45], [(*R*)-*N*-fluoroethyl-3-quinuclidinol]$PbBr_3$ [46] and [*R*-2-methylpiperidinium]PbI_3 [47]. However, in chiral lead-free OIMHSs, the research on dielectric switching is almost a wasteland waiting to be exploited in-depth.

Here, we synthesized a chiral lead-free tin(IV)-based OIMHS, namely $[R\text{-HQ}]_2SnCl_6$, which is composed of isolated inorganic skeletons $[SnCl_6]^{2-}$ and chiral organic cations $[R\text{-HQ}]^+$. It features a wide band gap of 4.11 eV. Furthermore, $[R\text{-HQ}]_2SnCl_6$ undergoes a phase transition at around 330 K (T_c) and shows a significant dielectric switching characteristic between high and low dielectric states around T_c. This work expands the chiral lead-free OIMHS family and throws light on the study of novel chiral lead-free OIMHS switching materials.

We dissolved (*R*)−3-quinuclidinol and $SnCl_4{\cdot}5H_2O$ in hydrochloric acid solution, then evaporated the solvent at 323 K to obtain $[R\text{-HQ}]_2SnCl_6$ single crystals (Supporting information). The crystal structure of $[R\text{-HQ}]_2SnCl_6$ was determined by single crystal X-ray diffraction measurement. The powder X-ray diffraction (PXRD) pattern (Fig. S1 in Supporting information) and the result of elemental analyses (Table S1 in Supporting information) confirm the phase purity of $[R\text{-HQ}]_2SnCl_6$. Meanwhile, the characteristic O–H (3494 cm^{-1}), N–H (3133 cm^{-1}), and -CH_2 (2959 cm^{-1}) peaks can be observed in the infrared (IR) spectrum of $[R\text{-HQ}]_2SnCl_6$ (Fig. S2 in Supporting information). At 273 K, $[R\text{-HQ}]_2SnCl_6$ crystallized in the chiral space group $P2_12_12_1$ (No. 19), belonging to the orthogonal system. The cell parameters are $a = 12.3677(2)$ Å, $b = 17.3397(3)$ Å, $c = 20.5796(4)$ Å, $\alpha = \beta = \gamma = 90°$, $V = 4413.34(14)$ $Å^3$ and $Z = 8$ (Table S2 in Supporting information). As shown in Fig. 1a and Fig. S3 (Supporting information), the asymmetric unit of $[R\text{-HQ}]_2SnCl_6$ is composed of four $[HQ]^+$ cations and two $[SnCl_6]^{2-}$ anions at 273 K. The four chiral $[HQ]^+$ cations show *R* configuration in $[R\text{-HQ}]_2SnCl_6$. Both the $[R\text{-HQ}]^+$ cation and the $[SnCl_6]^{2-}$ anion are ordered, and each Sn(IV) atom is coordinated with the surrounding six Cl atoms to form $[SnCl_6]^{2-}$ octahedra. Specifically, the Sn−Cl distances vary from 2.4160(9) Å to 2.4367(9) Å and 2.4172(9) Å to 2.4374(9) Å, and *cis*-Cl−Sn−Cl bond angles are in the range from 88.60(4)° to 92.10(4)° and 88.28(3)° to 91.95(4)° (Table S3 in Supporting information), showing the slight distortion. There are complex hydrogen bonds between $[R\text{-HQ}]^+$ cations and $[SnCl_6]^{2-}$ octahedra and between $[R\text{-HQ}]^+$ cations, including N-H···Cl, O-H···Cl, N-H···O and O-H···O hydrogen bonds. Details of the hydrogen bonds are shown in Fig. S3, and the average hydrogen bond length of N···Cl, O···Cl, N···O and O···O are 3.386 Å, 3.391 Å, 2.756 Å and 2.794 Å (Table S4 in Supporting information), respectively. For the packing structures of $[R\text{-HQ}]_2SnCl_6$, $[R\text{-HQ}]^+$ cations and $[SnCl_6]^{2-}$ anions are stacked with the interaction of hydrogen bonds, forming a three-dimensional hydrogen-bonded structure (Fig. 1b, Figs. S3 and S4 in Supporting information). It is noted that in typical OIMHSs, such as $[CH_3NH_3]PbI_3$, hydrogen bonding interaction exists only between the organic cation and the inorganic framework and there is only one kind of hydrogen bonding interaction like N-H···I hydrogen bonds [25,48]. However, in $[R\text{-HQ}]_2SnCl_6$, the organic cation $[R\text{-HQ}]^+$ links the inorganic $[SnCl_6]^{2-}$ octahedron through two kinds of hydrogen bonds N-H···Cl and O-H···Cl. Moreover, besides the hydrogen bonding interaction between the organic cation and the inorganic framework, there are also O-H···O and N-H···O hydrogen bonding interactions between the organic cations in $[R\text{-HQ}]_2SnCl_6$, distinct from that found in typical OIMHSs like $[CH_3NH_3]PbI_3$. As shown in Fig. S4, one $[R\text{-HQ}]^+$ cation containing the N4 atom connects with two $SnCl_6$ octahedra through N-H···Cl and O-H···Cl hydrogen bonds, respectively, to form a hydrogen-bonded trimer. Three adjacent hydrogen-bonded trimers then link the other three $[R\text{-HQ}]^+$ cations through hydrogen bonds respectively, in which the three $[R\text{-HQ}]^+$ cations are connected with O-H···O or N-H···O hydrogen bonds, resulting in a hydrogen-bonded layer. In this layer, the O1 atoms act as donors to further link $SnCl_6$ octahedra from adjacent hydrogen-bonded layers, which gives rise to a three-dimensional hydrogen-bonded structure (Fig. 1b and Fig. S4).

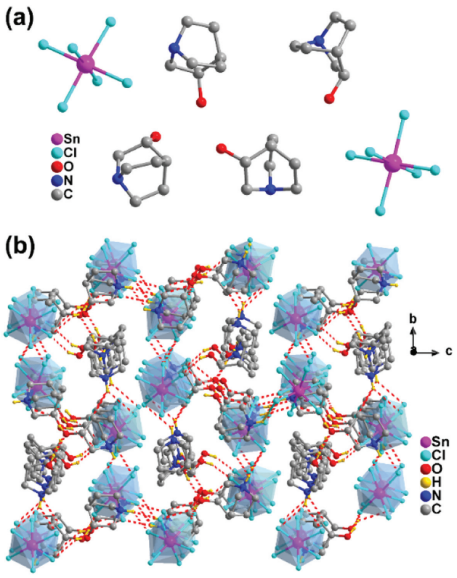

Fig. 1. (a) Asymmetric unit of $[R\text{-HQ}]_2SnCl_6$ at 273 K. (b) Packing views of $[R\text{-HQ}]_2SnCl_6$ at 273 K. Some hydrogen atoms are omitted for clarity. The dot lines denote hydrogen bonds.

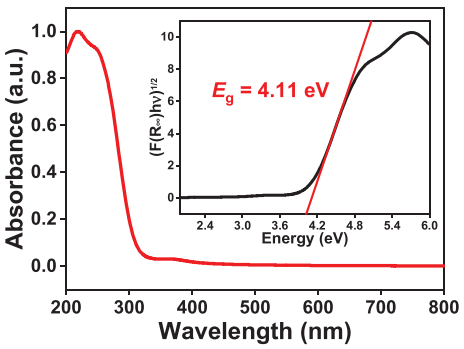

Fig. 2. UV–vis absorption spectrum of $[R\text{-HQ}]_2SnCl_6$. Inset: The *Tauc* plot.

The ultraviolet-visible (UV–vis) absorption spectrum was measured to get the optical bandgap. As depicted in Fig. 2, $[R\text{-HQ}]_2SnCl_6$ shows a broad absorption with an absorption edge up to 320 nm, conforming to the colorless crystals. The power law for the variation trend of absorption coefficient as a function of photo energy indicated an indirect bandgap feature, as found in other

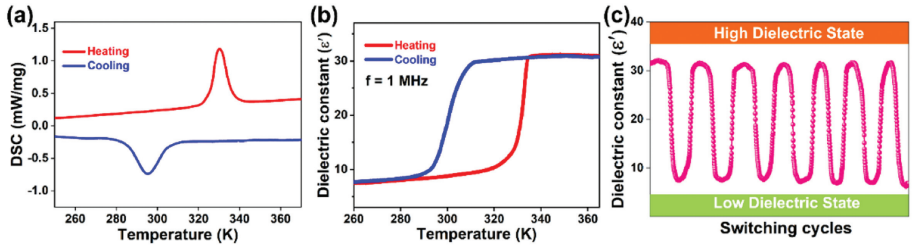

Fig. 3. (a) DSC curves of $[R\text{-HQ}]_2SnCl_6$. (b) The temperature-dependent real part (ε') of the dielectric constant of $[R\text{-HQ}]_2SnCl_6$ was measured at a frequency of 1 MHz upon heating and cooling. (c) Reversible switching of dielectric constant (ε') of $[R\text{-HQ}]_2SnCl_6$.

Sn(IV)-based OIMHS [(3-fluoro-*N*-methylbenzylamine)$_2SnCl_6$] [49]. The optical bandgap value of $[R\text{-HQ}]_2SnCl_6$ is estimated to be 4.11 eV from the *Tauc* equation, $(h\nu \cdot F(R_\infty))^{1/n} = A(h\nu - E_g)$, where h is the Planck constant, ν represents the frequency of vibration, $F(R_\infty)$ stands for the Kubelka-Munk function, and A is related to the proportional constant. Similar to other OIMHSs, the band gap of $[R\text{-HQ}]_2SnCl_6$ should also be mainly determined by its inorganic framework [48]. It is worth noting that the band gap of $[R\text{-HQ}]_2SnCl_6$ is larger than those of Pb-based chiral OIMHSs, such as [(*R*)-methylphenethylammonium]$_2PbCl_4$ ($E_g = 3.5$ eV) [50], [*R*/*S*-$C_6H_5CH(CH_3)NH_3$]$PbBr_3$ ($E_g = 3.30$ eV) [51] and [*R*/*S*-1-(4-chlorophenyl)ethylammonium]$_2PbI_4$ ($E_g = 2.34$ eV) [20], as well as Sb- and Bi-based chiral OIMHSs including [(*R*)−1-(4-fluoro)-phenylethylammonium]$_4[Bi_2Cl_{10}]$ ($E_g = 3.25$ eV) [22] and [(*R*)−1-(4-fluoro)-phenylethylammonium]$_4[Sb_2Cl_{10}]$ ($E_g = 3.35$ eV) [22]. Meanwhile, the band gap of $[R\text{-HQ}]_2SnCl_6$ is comparable to that of other Sn(IV) chloride-based OIMHSs such as $[(C_3H_5)_2N(CH_3)_2]_2SnCl_6$ ($E_g = 4.02$ eV) [52] and [(3-fluoro-*N*-methylbenzylamine)$_2SnCl_6$] ($E_g = 4.24$ eV) [49], which is due to that they have the similar $[SnCl_6]^{2-}$ inorganic frameworks that play the essential role in determining the band gap of OIMHSs. This makes $[R\text{-HQ}]_2SnCl_6$ have potential application in wide bandgap semiconductor-based devices.

One direct way to detect whether a compound has undergone a reversible temperature-triggered phase transition is to carry out differential scanning calorimetry (DSC) measurements to see if there are thermal anomalies during heating and cooling runs. As shown in Fig. 3a, the DSC was measured in the temperature range of 250−370 K. In the DSC curves of $[R\text{-HQ}]_2SnCl_6$, a pair of endothermic/exothermic peaks are exhibited at around 330 K/295 K in the heating and cooling runs (Fig. 3a), respectively, demonstrating that the occurrence of the reversible phase transitions at 330 K (T_c). The sharp shape of the endothermic/exothermic peaks and large thermal hysteresis up to ~35 K reveal a first-order phase transition. For convenience, the phase below T_c is labeled as the low-temperature phase (LTP), and the above T_c one is deemed to be the high-temperature phase (HTP). Notably, the $T_c = 330$ K of $[R\text{-HQ}]_2SnCl_6$ is in the range of desired moderate T_c (290−365 K) [53], which makes it work at both room temperature and slightly above room temperature without strict operating conditions.

The phase transition process is usually accompanied by dielectric anomalies. We then measured the temperature-dependent real part (ε') of the complex dielectric constant, at a frequency of 1 MHz upon heating and cooling. As shown in Fig. 3b, the ε' value increases slowly from 7.5 to 10 when heated to 320 K, corresponding to a low dielectric state. With the temperature further increasing to 345 K, the value of ε' has a large increase to 31.3. As the temperature continues to rise, the ε' of 31.3 remains almost unchanged, corresponding to a high dielectric state. The variation tendency of the ε' upon the cooling process shows a step-like change, which is similar to that upon the heating process, further strongly confirming the reversible phase transition. The dielectric switching contrast (the ratio of the ε' value between the high dielectric (31.3) and low dielectric (10) states) of $[R\text{-HQ}]_2SnCl_6$ was about 3.13. A high permittivity contrast is important for the practical application of dielectric switching materials [54]. Notably, the majority of recently reported OIMHS dielectric switching contrast on powder pressed tablets are below 3, such as (thiomorpholinium)$PbBr_3$ [49], (isoamylammonium)$_2PbCl_4$ [55] and [(*R*)-*N*-fluoroethyl-3-quinuclidinol]$PbBr_3$ [46], they undergo about 1.2-, 1.8- and 2.3-times dielectric changes near their T_c, respectively.

For $[R\text{-HQ}]_2SnCl_6$, during the heating-cooling process, these step-like dielectric changes that switch between different dielectric states also indicate the existence of dielectric bistable switching. The bistable state cycles test was conducted to explore the repeatability of the dielectric switching of $[R\text{-HQ}]_2SnCl_6$. As illustrated in Fig. 3c, with the temperature rising to above T_c, the ε' increase rapidly from the low dielectric state to the high dielectric state. Upon cooling, ε' decreases rapidly from the high dielectric state to a low dielectric state at around 295 K. The value of ε' is almost unchanged compared with the initial one even after 7 cycles of measurement, which further confirms that the dielectric switching has good repeatability. From all the above, the excellent dielectric switching characteristics of $[R\text{-HQ}]_2SnCl_6$ make it a good choice for exploring air-stable, thermally driven chiral lead-free dielectric switching OIMHSs.

To deeply understand the phase transition, the crystal structure in HTP deserves to be determined. For $[R\text{-HQ}]_2SnCl_6$, we were unable to successfully solve the HTP crystal structure despite repeated attempts, owing to the poor diffraction data. Fortunately, we gained the unit cell parameters from 273 K to 380 K in the heating process. At 343 K, the cell parameters are $a = 17.8396(11)$ Å, $b = 12.3772(7)$ Å, $c = 10.2262(6)$ Å, $\alpha = \beta = \gamma = 90°$, $V = 2258.0(2)$ Å^3 and $Z = 4$, which means it still belongs to the orthorhombic crystal system. As shown in Fig. 4a, the *a*- and *b*-axis lengths do not change much before and after the phase transition. However, its *c*-axis lengths and cell volume change abruptly around T_c, where the cell axis length and volume are halved, implying a first-order phase transition feature, which is consistent with the results of DSC. Consequently, it can be speculated that the number of $[R\text{-HQ}]^+$ cations in the asymmetric unit of structure in HTP is half that in LTP. To satisfy such a structural change, the $[R\text{-HQ}]^+$ cations would become disorder in the HTP. The order-disorder of organic $[R\text{-HQ}]^+$ cations may be responsible for the phase transition in $[R\text{-HQ}]_2SnCl_6$, as generally found in organic-inorganic hybrid phase transition materials [53,55-57]. In addition, we further performed variable-temperature PXRD measurements to confirm the structural phase transition of $[R\text{-HQ}]_2SnCl_6$ (Fig. 4b). As the temperature increased from 273 K to 313 K, the PXRD patterns remained unchanged. The temperature further rises to 353 K and above it, the diffraction peaks disappeared at 9.8°, 12.44°, 13.16°, 14.92°, 15.60°, 15.78°, 19.34°, and 19.96° in the pink dotted boxes. The apparent changes in PXRD patterns provide convincing evidence that $[R\text{-HQ}]_2SnCl_6$ undergoes a thermal-triggered phase transition. Besides, we also measured the PXRD patterns of $[R\text{-HQ}]_2SnCl_6$ when cool-

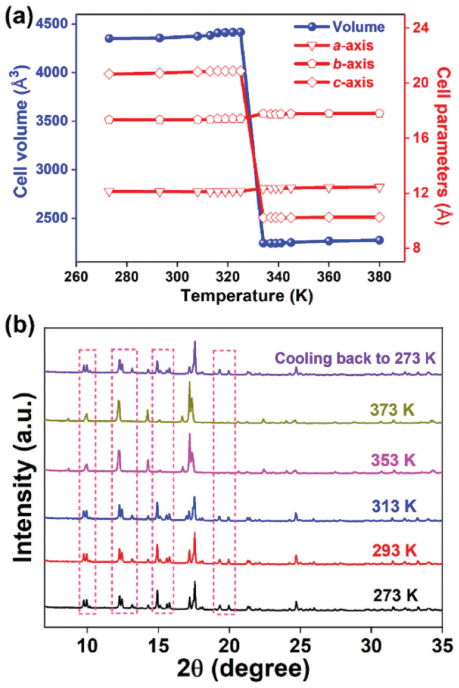

Fig. 4. (a) Temperature dependence of unit-cell parameters and (b) variable-temperature PXRD patterns of $[R\text{-HQ}]_2SnCl_6$.

ing back to 273 K, which match well with those obtained at the initial 273 K. This confirms the reversibility of the phase transition, which echoes the DSC and dielectric measurement results.

As the most studied OIMHSs, $CH_3NH_3PbI_3$ has excellent optoelectronic properties, but its air instability is an obstacle to its commercialization [58,59]. The phase stability and thermal stability of OIMHSs are crucial for their practical applications. We tested the phase stability and thermal stability of $[R\text{-HQ}]_2SnCl_6$, and analyzed them by PXRD studies and thermogravimetric analysis (TGA). We recorded the PXRD patterns of $[R\text{-HQ}]_2SnCl_6$ stored in the ambient atmosphere for one month, three months, and six months. Compared with the freshly prepared sample, the patterns of PXRD show no obvious change after half a year of air exposure (Fig. S5 in Supporting information), demonstrating the good phase stability of $[R\text{-HQ}]_2SnCl_6$. As shown in Fig. S6 (Supporting information), $[R\text{-HQ}]_2SnCl_6$ presents good thermal stability up to a high temperature of around 601 K.

In summary, we synthesized a new chiral lead-free Sn(IV)-based OIMHS, namely $[R\text{-HQ}]_2SnCl_6$ with a band gap of 4.11 eV. $[R\text{-HQ}]_2SnCl_6$ undergoes a reversible phase transition at around 330 K, verified by the DSC, dielectric measurements, and variable-temperature PXRD. Simultaneously, variable-temperature cell parameter analyses reveal that its *c*-axis length and cell volume are abruptly changed near T_c, where the crystal axis length and volume are halved, which strongly confirms the structural phase transition. Importantly, $[R\text{-HQ}]_2SnCl_6$ shows prominent dielectric switching characteristics between low and high dielectric states around T_c with good repeatability. In addition, it also demonstrates remarkable phase and thermal stability. We expect that by assembling more chiral organic cations into Sn(IV)-based OIMHSs, more novel high-performance chiral lead-free OIMHSs can be constructed.

Declaration of competing interest

The authors declare that they have no known competing financial interests or personal relationships that could have appeared to influence the work reported in this paper.

Acknowledgments

This work was supported by the National Natural Science Foundation of China (Nos. 22175082, 91856114 and 21703033).

Supplementary materials

Supplementary material associated with this article can be found, in the online version, at doi:10.1016/j.cclet.2022.107980.

References

[1] T.M. Brenner, D.A. Egger, L. Kronik, et al., Nat. Rev. Mater. 1 (2015) 15007.
[2] B. Saparov, D.B. Mitzi, Chem. Rev. 116 (2016) 4558–4596.
[3] F. Deschler, M. Price, S. Pathak, et al., J. Phys. Chem. Lett. 5 (2014) 1421–1426.
[4] C.C. Stoumpos, D.H. Cao, D.J. Clark, et al., Chem. Mater. 28 (2016) 2852–2867.
[5] Y. Dang, X. Liu, B. Cao, X. Tao, Matter 4 (2021) 794–820.
[6] G. Long, R. Sabatini, M.I. Saidaminov, et al., Nat. Rev. Mater. 5 (2020) 423–439.
[7] R. Naaman, Y. Paltiel, D.H. Waldeck, Nat. Rev. Chem. 3 (2019) 250–260.
[8] J. Ahn, E. Lee, J. Tan, et al., Mater. Horiz. 4 (2017) 851–856.
[9] V. Mujica, Nat. Chem. 7 (2015) 543–544.
[10] H. Lu, Z.V. Vardeny, M.C. Beard, Nat. Rev. Chem. 6 (2022) 470–485.
[11] G. Long, C. Jiang, R. Sabatini, et al., Nat. Photon. 12 (2018) 528–533.
[12] H. Lu, J. Wang, C. Xiao, et al., Sci. Adv 5 (2020) eaay0571.
[13] J.T. Lin, D.G. Chen, L.S. Yang, et al., Angew. Chem. Int. Ed. 60 (2021) 21434–21440.
[14] C. Chen, L. Gao, W. Gao, et al., Nat. Commun. 10 (2019) 1927.
[15] Y. Peng, X. Liu, L. Li, et al., J. Am. Chem. Soc. 143 (2021) 14077–14082.
[16] J. Song, T. Fang, J. Li, et al., Adv. Mater. 30 (2018) 1805409.
[17] Y. Dong, Y. Zhang, X. Li, et al., Small 15 (2019) 1902237.
[18] C.Q. Yuan, X.Y. Li, S. Semin, et al., Nano Lett. 18 (2018) 5411–5417.
[19] H.Y. Liu, H.Y. Zhang, X.G. Chen, R.G. Xiong, J. Am. Chem. Soc. 142 (2020) 15205–15218.
[20] C.K. Yang, W.N. Chen, Y.T. Ding, et al., Adv. Mater. 31 (2019) 1808088.
[21] H. Lu, C. Xiao, R. Song, et al., J. Am. Chem. Soc. 142 (2020) 13030–13040.
[22] N. Dehnhardt, M. Axt, J. Zimmermann, et al., Chem. Mater. 32 (2020) 4801–4807.
[23] L. Zhao, X. Han, Y. Zheng, et al., Adv. Photonics Res. 2 (2021) 2100056.
[24] S. Qi, F. Ge, X. Han, et al., Dalton Trans 51 (2022) 8593–8599.
[25] L. Yao, Z. Zeng, C. Cai, et al., J. Am. Chem. Soc. 143 (2021) 16095–16104.
[26] S. Liu, M.W. Heindl, N. Fehn, et al., J. Am. Chem. Soc. 144 (2022) 14079–14089.
[27] W. Shockley, H.J. Queisser, J. Appl. Phys. 32 (1961) 510–519.
[28] Z. Shi, J. Guo, Y. Chen, et al., Adv. Mater. 29 (2017) 1605005.
[29] C.R. Kagan, D.B. Mitzi, C.D. Dimitrakopoulos, Science 286 (1999) 945–947.
[30] X. Jiang, Z. Zang, Y. Zhou, et al., Acc. Mater. Res. 2 (2021) 210–219.
[31] F. Hao, C.C. Stoumpos, D.H. Cao, et al., Nat. Photon. 8 (2014) 489–494.
[32] J.P. Cao, F. Yan, Energy Environ. Sci. 14 (2021) 1286–1325.
[33] Y. Yua, P. Huang, Y. Wang, et al., Chin. Chem. Lett. 32 (2021) 3558–3561.
[34] B. Champagne, A. Plaquet, J.L. Pozzo, et al., J. Am. Chem. Soc. 134 (2012) 8101–8103.
[35] O. Sato, Nat. Chem. 8 (2016) 644–656.
[36] M. Wuttig, N. Yamada, Nat. Mater. 6 (2007) 824–832.
[37] R.G. Xiong, S.Q. Lu, Z.X. Zhang, et al., Angew. Chem. Int. Ed. 59 (2020) 9574–9578.
[38] K. Ariga, J.B. Li, J.B. Fei, et al., Adv. Mater. 28 (2016) 1251–1286.
[39] J.Y. Liu, S.Y. Zhang, Y. Zeng, et al., Angew. Chem. Int. Ed. 57 (2018) 8032–8036.
[40] M. Salinga, M. Wuttig, Science 332 (2011) 543.
[41] R. Shang, S. Chen, B.W. Wang, et al., Angew. Chem. Int. Ed. 55 (2016) 2097–2100.
[42] S. Deng, J. Li, X. Chen, et al., Chin. Chem. Lett. 31 (2020) 1686–1689.
[43] Y. Xue, Z. Zhang, P. Shi, et al., Chin. Chem. Lett. 32 (2021) 539–542.
[44] M. Yang, H. Cheng, Y. Xu, M. Li, Y. Ai, Chin. Chem. Lett. 33 (2022) 2143–2146.
[45] C. Su, M. Lun, Y. Chen, et al., CCS Chem. 3 (2021) 2021–2031.
[46] Y. He, Z. Chen, X. Chen, et al., Mater. Chem. Front. 6 (2022) 1292–1300.
[47] H. Peng, Y.H. Liu, X.Q. Huang, et al., Mater. Chem. Front. 5 (2021) 4756–4763.
[48] S. Liu, L. He, Y. Wang, et al., Chin. Chem. Lett. 33 (2022) 1032–1036.
[49] X.L. You, J.T. Yao, Z.H. Wei, Dalton Trans. 49 (2020) 7252–7257.
[50] X. Zhang, W. Weng, L. Li, et al., Small 17 (2021) 2102884.
[51] Y. Dang, X. Liu, Y. Sun, et al., J. Phys. Chem. Lett. 11 (2020) 1689–1696.
[52] S. Yan, W.T. Chen, S.X. Ouyang, et al., J. Phys. Chem. C 123 (2019) 9364–9370.
[53] B. Huang, L.Y. Sun, S.-S. Wang, et al., Chem. Commun. 53 (2017) 5764–5766.
[54] M. Maczka, A. Nowok, J.K. Zareba, et al., ACS Appl. Mater. Interfaces 14 (2022) 1460–1471.
[55] X.Q. Huang, H. Yu, Z.K. Xu, et al., Inorg. Chem. 60 (2021) 16871–16877.
[56] M. Ksiadzyna, A. Gagor, A.M. Bisiorek, et al., J. Mater. Chem. C 7 (2019) 10360–10370.
[57] P.F. Li, W.Q. Liao, Y.Y. Tang, et al., Proc. Natl. Acad. Sci. U. S. A. 116 (2019) 5878–5885.
[58] G. Divitini, S. Cacovich, F. Matteocci, et al., Nat. Energy 1 (2016) 15012.
[59] H. Zhou, Q. Chen, G. Li, et al., Science 345 (2014) 542–546.